

Accepted for publication in Journal of Geophysical Research. Copyright 1999 by the American Geophysical Union. Further electronic distribution is not allowed.

Langley method of calibrating UV filter radiometers

James Slusser,¹ James Gibson,¹ David Bigelow,¹ Donald Kolinski,^{1,2} Patrick Disterhoft,³ Kathleen Lantz,³ and Arthur Beaubien⁴

Abstract. The Langley method of calibrating UV multifilter shadow band radiometers (UV-MFRSR) is explored in this paper. This method has several advantages over the traditional standard lamp calibrations: the Sun is a free, universally available, and very constant source, and nearly continual automated field calibrations can be made. Although 20 or so Langley events are required for an accurate calibration, the radiometer remains in the field during calibration. Difficulties arise as a result of changing ozone optical depth during the Langley event and the breakdown of the Beer-Lambert law over the finite filter band pass since optical depth changes rapidly with wavelength. The Langley calibration of the radiometers depends critically upon the spectral characterization of each channel and on the wavelength and absolute calibration of the extraterrestrial spectrum used. Results of Langley calibrations for two UV-MFRSRs at Mauna Loa, Hawaii were compared to calibrations using two National Institute of Standards and Technology (NIST) traceable lamps. The objectives of this study were to compare Langley calibration factors with those from standard lamps and to compare field-of-view effects. The two radiometers were run simultaneously: one on a Sun tracker and the other in the conventional shadow-band configuration. Both radiometers were calibrated with two secondary 1000 W lamp, and later, the spectral response functions of the channels were measured. The ratio of Langley to lamp calibration factors for the seven channels from 300 nm to 368 nm using the shadow-band configuration ranged from 0.988 to 1.070. The estimated uncertainty in accuracy of the Langley calibrations ranged from $\pm 3.8\%$ at 300 nm to $\pm 2.1\%$ at 368 nm. For all channels calibrated with Central Ultraviolet Calibration Facility (CUCF) lamps the estimated uncertainty was $\pm 2.5\%$ for all channels.

1. Introduction

Accurate calibration of ground-based ultraviolet (UV) radiometers is crucial in identifying trends in UV radiation [Bigelow *et al.*, 1998], developing UV climatologies, and quantifying the amount of shortwave radiation absorbed by clouds and aerosols [Kiedron *et al.*, 1999]. The Langley method of calibrating UV shadow-band radiometers (UV-MFRSRs) using the Sun as the irradiance source is explored in this paper. In addition, we investigated how effectively the shadow-band radiometer retrieves the direct beam by comparing Langley calibration factors, retrieved using the radiometer in both shadow-band and tracker configurations with factors derived from standard lamps.

Calibrations of UV and visible (VIS) radiometers are currently performed using 1000 W FEL-type secondary standard lamps traceable to the National Institute of Standards and Technology (NIST) [Early *et al.*, 1998a]. The secondary standard lamps, typically used in the horizontal position, have an absolute uncertainty ranging from $\pm 1.0\%$ to $\pm 0.8\%$ in the wavelength range from 300 nm to 380 nm, respectively [Early *et al.*, 1998b]. The lamps cost over \$20,000 with the necessary power supplies, are fragile, and have a lifetime of about 50 hours. By contrast the spectral irradiance of the Sun between 300 nm and 400 nm is constant to within 0.5% over the 11 year solar cycle [Lean *et al.*, 1997] and is free and universally available to all researchers. Thus

the relative uncertainty of lamps in this wavelength region is somewhat larger than the possible instability of the Sun. This gives reason to believe the Sun is superior to lamps as an irradiance source were it not for the intervening atmosphere of the Earth. Variability of the atmospheric transmission during the period of a Langley measurement, especially in the UV, is typically the limiting factor in the accuracy possible using this method [Schmid *et al.*, 1998]. To minimize the effects of changes in atmospheric transmission, measurements using two U.S. Department of Agriculture (USDA) UV-MFRSRs were made during 7 months in 1998 under the exceptionally clear and stable skies at Mauna Loa Observatory (MLO) Hawaii, at elevation 3.4 km.

The accuracy of Langley calibration of the radiometers depends critically upon the spectral characterization of each channel and on the wavelength and absolute calibration of the extraterrestrial spectrum being used. As more accurate satellite measurements of the extraterrestrial solar irradiance become available, Langley calibrations can be revised. Finally, the Langley method allows for a continuous calibration check to give an upper limit on radiometer stability, which is affected by the stability of the diffuser, filter, photodiode, and electronics [Bigelow and Slusser, this issue]. These automated in situ measurements require no break in the time series. It is rather time consuming to produce enough events for a Langley calibration (about 20 or so are required), and this may take several months at turbid sites. However, Harrison and Michalsky [1994] report 143 Langley events using a VIS-MFRSR during 14 months at the less than ideal site of Boulder, Colorado, and Bigelow and Slusser [this issue] report similar statistics in the UV in NE Colorado.

This paper is arranged as follows: Section 2 outlines the basic theory of the Langley method. Section 3 briefly reviews previous work, and section 4 summarizes the instrumentation used in this experiment. Section 5 sets out the corrections applied to obtain Langley calibrations. Section 6 presents a comparison of Langley and lamp calibration factors, including a discussion of field-of-view effects, while section 7 discusses the sources of uncertainty. Finally, section 8 provides a summary and conclusions.

2. Theory

The attenuation of the Sun's direct-beam monochromatic radiation passing through the Earth's atmosphere is described by the Beer-Lambert law

$$I_{\lambda} = R^2 I_{o,\lambda} \exp(-\sum \tau_{\lambda,i} m_i), \quad (1)$$

where I_{λ} is the direct normal irradiance at the ground at wavelength λ , R is the Earth-to-Sun distance in astronomical units (AU) at the time of measurement, $I_{o,\lambda}$ is the extraterrestrial irradiance, $\tau_{\lambda,i}$ is the optical depth for the i th scatterer or absorber, and m_i is the air mass of the i th scatterer or absorber through the atmosphere [Thomason *et al.*, 1983]. Taking the natural log of both sides,

$$\ln I_{\lambda} = \ln (R^2 I_{o,\lambda}) - \sum m_i \tau_i \quad (2)$$

For the uncalibrated voltages measured by the detector the equation is

$$\ln V_{\lambda} = \ln (R_2 V_{o,\lambda}) - \sum m_i \tau_i \quad (3)$$

where V_{λ} is the measured voltage of a particular channel, and $V_{o,\lambda}$ is the extrapolated voltage intercept at zero air mass. This is the voltage the detector would measure outside the Earth's atmosphere at 1 AU oriented normal to the Sun.

Calibrated global irradiance over the filter passband $I_{\lambda,F}$ is obtained by multiplying the detector global voltage measured at the ground V_{λ} by the calibration factor k . This factor k [Bigelow *et al.*,

1998] is determined using the voltage intercept $V_{o,\lambda}$, the extraterrestrial solar irradiance $I_{o,\lambda}$ (D. Prinz, personal communication, 1997), corrected for the vacuum to air wavelength shift based on the index of refraction of dry air [Houghton, 1985], and the spectral response function (SRF) of the filter/photodiode combination F_λ .

$$I_{\lambda,F} = V_\lambda k = \frac{V_\lambda \int I_{o,\lambda} F_\lambda d\lambda}{V_{o,\lambda} \int F_\lambda d\lambda} \quad (4)$$

This assumes that the direct and diffuse components of the voltage have been corrected for an ideal cosine angular response. In fact, the direct component of the voltage has been cosine corrected on the basis of laboratory characterizations, but the diffuse component has not. Using the isotropic sky radiance assumption [Gröbner *et al.*, 1996] and the measured angular response of the detector, this will cause a bias of less than $\pm 3\%$ in the global (direct plus diffuse horizontal) irradiance for all channels. Another assumption inherent in Langley calibration is linearity of the detectors' response to the irradiance intensity, which is that doubling the irradiance results in doubling the voltage.

Thomason *et al.* [1983] note that since the concentration of absorbers and scatterers (ozone, air molecules, and aerosols) have different altitude concentration profiles, the air mass factor must be calculated separately for each. The concentration of air molecules falls off exponentially, while ozone has its largest concentrations at an elevation of about 20 km. Aerosols are usually concentrated below 3 km except in cases of extreme stratospheric loading after a major volcanic eruption. Tomasi *et al.* [1998] computed air mass factors for various gaseous absorbers at solar zenith angles (SZAs) from 0° to 87° .

The range of air mass factors at a given wavelength suitable for Langley plots is governed by the sum of the products of the optical depths τ_i and the individual air mass factor m_i (the second term on the right hand side of Equation (3)). Extinction of the direct beam is much larger in the UV than in the visible region of the spectrum. This is the result of both the strong absorption due to ozone and the molecular Rayleigh scattering, which increases approximately as λ^{-4} , resulting in a combined optical depth exceeding 3.0 at 300 nm. Current state-of-the-art solid-state detectors are limited to not more than four decades of dynamic range. Therefore the range of air masses appropriate for UV Langley plots is more restricted than for the visible, where at 415 nm, the total optical depth is typically less than 0.5. After a number of ranges were tried, an air mass range of 1.2 to 2.2 (SZA of 33.6° to 63.0°) was determined to be suitable for the UV instead of the range of 2 to 6 (SZA 60.0° to 80.4°) commonly used in the visible part of the spectrum [Harrison and Michalsky, 1994]. At a molecular air mass of 2.2 the ratio of ozone air mass factor m_o to the Kasten and Young [1989] molecular air mass m_m is 1.008 [Tomasi *et al.*, 1998]. Assuming a column ozone amount of 300 Dobson units (DU), using the same air mass for m_o as for m_m would cause a bias in the Langley voltage intercept $V_{o,\lambda}$, ranging from about +4.6% at 300 nm to 0% at 368 nm.

Extrapolations to zero air mass voltages $V_{o,\lambda}$ in the UV are more variable than those in the visible region as a consequence of the diurnal variations in the ozone and to a smaller extent aerosol optical depth and rapid attenuation of the UV direct beam with increasing air mass. Large changes in ozone optical depth in the Hartley-Huggins band below 320 nm over the finite 2.0 nm passband of the UV-MFRSR result in the failure of the Beer-Lambert law, adding to the uncertainty of the Langley-derived calibrations [Wilson and Forgan, 1995]. Since the shorter wavelengths are attenuated more strongly than the longer wavelengths as the SZA or column ozone increases, the effective center wavelength of the passband shifts to the red. Further

complications result from the larger fraction of diffuse light in the field of view around the Sun's disk due to molecular scattering at these shorter UV wavelengths [Tüg and Bauman, 1994; McKenzie and Johnston, 1995]. Correction factors for these problems are discussed in section 5.

3. Previous Work

Shaw [1982] set a 10 channel Sun-tracking filter radiometer with center wavelengths from 383 to 1010 nm atop MLO for 1 year to study variations in the spectral output of the Sun and in atmospheric transmission. Extrapolations of the zero air mass voltages for 132 days of observations had a standard deviation of between 0.3% at 789 nm and 1.2% at 383 nm. He notes that the large uncertainties in the absolute calibration of the extraterrestrial irradiance available at that time limited the use of the Langley method for absolute calibration.

Schmid and Wehrli [1995] and Schmid *et al.* [1998] discuss the methodology of obtaining Langley calibrations in the region between 300 and 1025 nm using a 13 channel Sun-tracking filter radiometer with a 2.8° full field of view. At the two shortest UV wavelengths, 300 nm and 305 nm, the authors report that Langley plots were highly nonlinear and suggest out-of-band "red-light" leakage as the reason. At 313 nm the standard deviation (1σ) of zero air mass voltages for 17 events at Mount Lemmon, Arizona, was 2.4%, contributing to an estimated total uncertainty in the calibration factor of $\pm 6.1\%$. Wilson and Forgan [1995] describe a procedure to calibrate a UV spectrometer using a Langley-calibrated filter radiometer at 368 nm as a transfer standard. Their method includes corrections for the angular response of the detector to the diffuse and direct-beam radiation.

4. Instrumentation

The USDA UV Radiation Monitoring Program [Bigelow *et al.*, 1998] makes measurements at 26 U.S. sites using the Yankee Environmental Systems (YES, Turners Falls, Massachusetts) UV-MFRSR. The measurements are made every 20 s and combined to 3 min averages. The impact of calculating the air mass at the time midpoint of 5 min averages at an air mass of 2 to 6 results in an error in V_o of 0.18% [Harrison and Michalsky, 1994]. Using the air mass at the time midpoint of 3 min averages over the air mass range from 1.2 to 2.2 used in the UV in this study would result in even smaller errors in $V_{o,\lambda}$. The UV-MFRSR [Bigelow *et al.*, 1988] is a seven channel ultraviolet version of the visible multifilter rotating shadow-band radiometer described by Harrison *et al.* [1994]. This new shadow-band instrument contains separate solid-state detectors each with nominal 2 nm full width at half maximum (FWHM) ion-assisted-deposition interference filters at 300, 305, 311, 318, 325, 332, and 368 nm nominal center wavelengths. The 368 nm wavelength is a standard (WMO) wavelength, and the others except 300 nm are close to Dobson wavelengths. The 300 nm channel was chosen as the shortest wavelength where sufficient signal-to-noise was achievable. Each detector shares a common diffuser, thereby allowing total horizontal (no blocking) and diffuse horizontal (direct beam blocked by the shadow band) irradiance to be measured simultaneously at each passband. Direct normal irradiance is derived in near real time by firmware included within the data logging component of the instrument. Harrison *et al.* [1994] describe the corrections applied in retrieving the direct beam by the subtraction of the diffuse horizontal from the total horizontal irradiance. All three measurements are returned for each 3 min interval.

5. Corrections Applied

Two corrections are needed to obtain UV Langley calibrations: one for finite band pass of the filter and the other for the ozone air mass factor. The first, made because the ozone cross section at wavelengths shorter than 320 nm changes rapidly with wavelength, is a correction factor applied to each instantaneous detector voltage. These factors, which correct the 2.0 nm FWHM radiometer data to simulate monochromatic direct irradiance, were calculated using the SRF of the filters and direct solar irradiance from a model. A discrete-ordinate radiative transfer model (DISORT) [Stamnes et al., 1988], with a new interface TUV V3.8 [Madronich, 1993] was used to calculate the ratio of the direct irradiance at the peak of the filter function $I_{\text{dir}}(\lambda_o, m)$ to the product of SRF of the filters $F(\lambda)$ and the direct irradiance $I_{\text{dir}}(\lambda, m)$. This calculation was repeated over a range of air masses from 1.2 to 2.2 with an ozone column of 300 DU to generate correction factors $c(m, \lambda_o)$ for each filter:

$$c(m, \lambda_o) = \frac{I_{\text{dir}}(m, \lambda_o)}{\int I_{\text{dir}}(\lambda) F(\lambda) / (\int F(\lambda) d\lambda)}. \quad (5)$$

For the modest variations in column ozone normally encountered at MLO (250 to 320 DU) it was found to be sufficient to make the corrections for a fixed ozone amount of 300 DU. Every voltage V_λ for each day's Langley plots was then multiplied by the appropriate factor at its center wavelengths before the $V_{o,\lambda}$ was computed. The approximate overall magnitude of these bandwidth corrections for a column ozone of 300 DU is shown in Table 1.

The second correction to the Langley plots accounted for the difference between the ozone air mass factor m_o and the molecular air mass factor m_m . Using equation (3), $V_{o,\lambda}$ was computed at each channel's center wavelength using the molecular air mass factors m_m for each m_i term for a range in air mass from 1.2 to 2.2. Then $V_{o,\lambda}$ was recomputed at the same wavelength (called $V'_{o,\lambda}$) using the ozone air mass m_o from Komhyr [1980] for the ozone term and the molecular air mass m_m for the aerosol and molecular terms. The ratio of ($V_{o,\lambda} / V'_{o,\lambda}$) constituted the correction factor for a given channel. Each average $V_{o,\lambda}$ was multiplied by this factor. The magnitude of the corrections due to the ozone air mass factor are found in Table 1.

Another method of determining $V_{o,\lambda}$, which accounts for the different air mass factors of molecules, ozone, and aerosols, is to regress $\ln(V_\lambda)$ against the reduced or weighted air mass factor m_{red} described by Forgan [1988] where

$$m_{\text{red}} = \frac{\sum_{i=1}^n m_i \tau_i}{\sum_{i=1}^n \tau_i}. \quad (6)$$

For the limited range of air mass factors used in this study, the correction factor developed in the preceding paragraph was found to be satisfactory.

6. Comparison of Langley to Lamp Calibrations

6.1. Langley Calibrations

Langley calibration factors for two UV-MFRSR radiometers, YES serial numbers 282 and 393, were obtained at MLO (3.4 km elevation) as follows. The two radiometers were set up in either of two configurations: one had the shadow-band removed and was placed on a Sun tracker with a collimated full field of view of either 2.0° or 1.5° , the other was in the conventional shadow-band

configuration. Only morning values were used because the afternoons are more often cloudy and have a larger and more variable aerosol concentration [Shaw, 1982]. For the entire experiment from January 1 to September 30, 1998, a total of 137 Langley plot voltage intercepts $V_{o,\lambda}$ s at 300 nm for radiometer 282 were computed using the objective algorithm of Harrison and Michalsky [1994] and for radiometer 393, a total of 163 plots were obtained. The criteria of a successful Langley plot was a minimum of one-third points with a standard deviation around the regression line of less than 0.009. Table 2 shows the configuration of the radiometers and the number of Langley plots at 300 nm for the three periods of measurement. Voltage intercepts $V_{o,\lambda}$ values, with standard deviations $> \pm 2 \sigma$ from the mean were removed from the analysis. The total number of acceptable Langley plots for the entire experiment and the number of outliers for each instrument and channel is shown in Table 3.

In the initial setup the two radiometers were run simultaneously from January 1 to February 25, 1998. For radiometer 282 there were 45 Langley plots, and for radiometer 393, a total of 50 Langley plots were obtained at 300 nm. An average Langley calibration factor was obtained for each instrument using equation (4). On February 27 the two instruments were swapped, so the radiometer that was on the tracker came back to the shadow-band mode and vice versa. The radiometers were run together until April 28 resulting in 41 Langley plots for radiometer 282 and 31 Langley plots for radiometer 393 at 300 nm. Again, average Langley calibration factors were obtained. For these first two periods the tracker field of view was 2.0° . On April 29 the two radiometers were sent back to the Central Ultraviolet Calibration Facility (CUCF) in Boulder, Colorado, where lamp calibrations were performed on May 15. From June 28 to September 30 the radiometers were again run in parallel in the same positions as on March 1; however, the tracker field of view was reduced to 1.5° . During this last period there were 71 Langley plots for radiometer 282 and 56 plots for radiometer 393 at the 300 nm channel.

A Langley plot for the 300 nm of radiometer 282 in the shadow-band configuration taken on March 1, 1998, is shown in Figure 1. During the 213 days radiometer 282 was in the standard shadow-band configuration, the drift (as determined by fitting a least squares line through the voltage intercepts) ranged from 0.1% to 1.3%, as shown in Table 4. Tables 5 and 6 show the average $V_{o,\lambda}$ and percent standard deviations for radiometers 393 and 282, respectively, for the three periods of measurement. The percent standard deviations, σ , range from 4.4% at 300 nm to 1.1% at 368 nm. The standard errors of the mean (σ / \sqrt{N}) are much smaller, ranging from 0.8% at 300 nm to 0.1% at 368 nm.

6.2. Field-of-View Effect

One of the objectives of the experiment was to determine how effectively the shadow band retrieves the direct beam by comparing Langley calibration factors retrieved using both the shadow band and the tracker results with those from conventional lamps. Figure 2 shows the geometry of the collimating tube. The tube was lined with black felt paper to eliminate internal reflections. The MLO tracker holds tracking to within 0.1° . The image of the Sun overfilled the radiometer diffuser with an annulus of a width of about 2 mm. After all the Langley calibration factors were computed, as shown below, using the results from the tracker and the shadow band, it was determined that the best agreement with lamp calibration factor results ensued using the shadow-band results.

It is instructive to compare the ratio of Langley calibration factors to the average of the two lamp calibration factors. For radiometer 282 (Figure 3), which had a 2° field-of-view on the tracker before its extended stay as a shadow band, there is no

significant difference between the ratio of calibration factors derived in the shadow-band mode and those derived when the radiometer was on the tracker. Radiometer 393 (Figure 4) was first in the shadow-band mode, then on the tracker with a field of view of 2.0° , and finally on the tracker with a field of view of 1.5° . Again, there are no major differences between factors derived with the radiometer in the shadow-band configuration and those from the tracker except at 300 nm. Thus it can be concluded that the Langley calibration factors retrieved in the shadow-band mode are equivalent to those on the Sun tracker within the expected statistical error except for the unexplained anomaly for radiometer 393 at 300 nm.

6.3. Lamp Calibrations

The radiometers were calibrated at the CUCF in Boulder, Colorado on May 15, 1998, using two different lamps. This calibration consisted of mounting the radiometers in the portable field calibration system [Early *et al.*, 1998] which employs a machined adapter plate specific for the UV-MFRSR. This system positions a 1000 W FEL-type secondary standard lamp 50.0 cm from the top surface of the radiometer's diffuser. These secondary standard lamps were produced by the CUCF using a dedicated system to measure absolute irradiance, accomplished by using the average of three NIST-calibrated primary traveling standards. The two secondary lamps used for the calibrations were 96598 and 96599, which both have a stable calibration and operation history.

The SRFs of each channel of the radiometers (measured through the diffuser, filter, photodiode, and preamplifier) were characterized several months later on October 10, 1998, at the CUCF using a 300 W Cermox xenon arc lamp (model LX 300 UV, ILC, Sunnyvale, California) dispersed through a 1.0 m double monochromator (model U-1000, Instruments SA, Edison, New Jersey) with a resolution of 0.2 nm. To obtain the calibration factor in ($W / m^2 / nm / V$), the standard 1000 W lamp irradiances were interpolated onto a 0.1 nm grid and the SRF passed over these irradiances and divided by the voltage of each channel while under illumination.

The comparisons between the Langley and the CUCF lamp calibration factors are shown in Table 7 for radiometer 282 and Table 8 for radiometer 393. The ratios of the Langley to lamp calibration factors are shown in Table 9 for radiometer 282 and in Table 10 for radiometer 393. For radiometer 282 the ratio of the Langley to lamp calibrations ranged from 0.997 at 305 nm to 1.032 at 332 nm. For radiometer 393 the range of the ratio of Langley to lamp calibrations was 0.988 at 325 nm to 1.070 at 300 nm.

7. Uncertainty Analysis

7.1 Uncertainty in Langley Calibration Factors

When assigning uncertainty to the calibration factors determined in this study, it is important to distinguish between the absolute accuracy appropriate for irradiance comparisons and the repeatability that is suitable for determining irradiance trends at a given site. The sources of uncertainty for both absolute accuracy and repeatability of the Langley calibration factors are listed in Table 11. The uncertainty of the extraterrestrial irradiance does not factor into the repeatability uncertainty. For the uncertainty of $V_{o,\lambda}$ values we used the standard error of the mean [Barlow, 1989], which is justified with a Gaussian distribution of $V_{o,\lambda}$ values. Figure 5 shows the distribution of the 133 $V_{o,\lambda}$ values made between March 1 and September 30, 1988, for radiometer 282 in the shadow-band mode. A Gaussian distribution has been overlain over the histogram, which demonstrates the Gaussian distribution is well approximated. The uncertainty of the $V_{o,\lambda}$ values is also the largest at the shortest wavelengths. Assuming that the instantaneous voltages from the channels during the Langley event are repeatable,

the uncertainty in $V_{o,\lambda}$ values is limited by the constancy of the atmospheric transmission during the time of the Langley event. The gain of each channel has been optimized for the spectral distribution and typical irradiance levels of the sunlight reaching the ground, so repeatability of the instantaneous voltages is excellent for this experiment and is not included in the uncertainty budget. Operating at MLO minimizes changes in transmission because of the exceptionally low turbidity and, since the site is subtropical, the very slow variations in column ozone. Increasing the number of observations reduces the uncertainty since the standard error of the mean is reduced in proportion to $(1/\sqrt{n})$, where n is the number of observations. The somewhat larger uncertainties at the shortest wavelengths could also be reduced by limiting Langley events to those days when ozone and aerosol optical depths are more constant.

Out-of-band light resulted in no useful Langley plots 300 nm and 305 nm for *Schmid et al.* [1998] but is not a problem for the current experiment. All channels are “red-blind,” i.e., have no spectral response to wavelengths for $\lambda > 380$ nm, confirmed by *Bigelow et al.* [1998] who report measurements of integrated red-light leakage over all wavelengths at all channels for the UV-MFRSR of $<0.5\%$ for irradiances at $SZA = 45^\circ$. In fact, since the Langley plot in Figure 3 is still linear at 63° (at an air mass of 2.2) with an order of magnitude less light, the out-of-band rejection must be better than the result just quoted. The estimated uncertainty caused by out-of-band leakage is $<0.2\%$ and has not been included in the uncertainty budget.

The corrections made for finite bandwidth and ozone air mass, described in section 5, are largest for the shortest wavelengths where these corrections also have the largest uncertainties. At the shortest wavelengths the uncertainty of both the accuracy and the repeatability is dominated by the finite bandwidth correction. At 300 nm it was estimated that the bandwidth correction introduced an uncertainty of about $\pm 3\%$. This error could be reduced by repeating the calculation for various ozone amounts and making the correction ozone specific. Similarly, the correction for ozone air mass factors, which contributes 1.0% at 300 nm, could be made explicitly for each measurement [*Schmid et al.*, 1998]. Such a calculation would require knowledge of the column ozone amount for each Langley event, which is readily obtained from the global irradiance of the UV-MFRSR [*Slusser et al.*, 1998]. This would reduce the magnitude of this uncertainty.

The absolute irradiance uncertainty of the extraterrestrial solar irradiance, including wavelength alignment, contributes only to the uncertainty accuracy. This uncertainty is estimated at $\pm 2.0\%$ and is subject to much the same uncertainty as these radiometers calibrated using standard lamps. This uncertainty will be reduced in the future as the uncertainty is reduced in primary lamp calibrations for satellites that measure the extraterrestrial solar irradiance. When more accurate determinations of the extraterrestrial solar irradiance become available, Langley calibration factors can be revised. Since the solar irradiance is known to have variations of $<0.5\%$, a 0.5% uncertainty in this parameter was assigned for repeatability.

Finally, the wavelength repeatability of the 1.0 m spectrometer used to characterize the SRF of the radiometers was measured by the CUCF to be ± 0.02 nm, which results in an uncertainty of about $\pm 0.5\%$ in the Langley calibration factor. The wavelength repeatability was measured by repeatedly observing the position of the centroid of the 253.65 nm Hg line. Thus the wavelength uncertainty in the SRF of the radiometer is a small contribution to the overall uncertainty budget.

Assuming these uncertainties are randomly distributed and independent, they may be combined using the root mean method [*Barlow*, 1989]. The total uncertainty in absolute accuracy at 300 nm is $\pm 3.8\%$ using the standard error of the mean for the uncertainty in $V_{o,\lambda}$. The uncertainty in repeatability at 300 nm is

estimated at $\pm 2.1\%$. At 332 nm and 368 nm the accuracy uncertainty is $\pm 2.1\%$, using the standard deviation of the mean for $V_{o,\lambda}$. The total uncertainty in repeatability is $\pm 0.7\%$ at 332 nm and 368 nm.

7.2. Uncertainty in Lamp Calibration Factors

Table 12 summarizes the errors associated with the lamp calibrations. The absolute uncertainty of the NIST-traceable secondary standard is estimated from $\pm 1.0\%$ at 300 nm to $\pm 0.8\%$ at 380 nm [Early *et al.*, 1998b]. We have approximated this to $\pm 1.0\%$ at all wavelengths.

Kiedron *et al.* [1999] have made a study of lamp-to-lamp comparability in the visible region of the spectrum, but to the authors' knowledge no such study has been published in the UV. Uncertainties due to cubic spline interpolation of the NIST irradiance reported every 10 nm onto a 0.1 nm wavelength grid are about $\pm 0.4\%$ and dark voltage subtraction uncertainties are $\pm 1.0\%$. The same wavelength uncertainty determined above for the SRF leads to an uncertainty of $\pm 0.5\%$ for all channels.

While the lamps have a $\pm 1.0\%$ accuracy, the voltages from the radiometer channel during lamp calibration are not so repeatable. For the very low light levels incident on the radiometer channels during lamp calibrations, the high-impedance amplification circuits, optimized for the typical range of solar irradiances reaching the ground, approach the detection limit. Figure 6 shows the significant difference in irradiance from lamp 96599 and a solar irradiance spectrum generated using DISORT for MLO (column ozone=280 DU, SZA=63°, altitude=3.4 km, $\tau_{\text{aer}}=0.05$, surface albedo=0.02). The 300 nm and 305 nm channels, which have extremely high gain to account for the extremely small solar irradiances, have adequate signal to noise under lamp calibrations. The 311 nm and longer-wavelength channels, having lower gains optimized for the larger solar irradiances at the longer wavelengths, generate lower voltages under lamp calibrations because the lamp irradiance at these wavelengths is 2 orders of magnitude weaker than the typical solar irradiance. It is important to note that these same channels receive sufficient irradiance for good signal to noise during the Langley plot resulting in excellent repeatability. Superior signal to noise constitutes a major advantage of the Langley calibration method over lamp calibrations in the UV. The ratio of lamp calibration factors for the same radiometer using two NIST traceable lamps (Tables 9 and 10) range from 0.999 to 1.050, which is outside of the stated accuracy of the individual lamps. The reason for these differences is the poor repeatability of the 311 nm and the longer-wavelength channel voltage under lamp calibration. An error of $\pm 2.0\%$ has been assigned to the voltage repeatability measured from the detector. Propagating these independent uncertainties leads to an overall estimated uncertainty of $\pm 2.5\%$ for all channels.

8. Conclusions

The Langley and lamp calibration factors from the two lamps agree to within their combined uncertainties for all channels of radiometer 282. For radiometer 393 using lamp 96598 the ratios are slightly larger than the combined uncertainties, but only one channel is outside the uncertainties using lamp 96599. We suspect an insufficient warm-up period for this radiometer is the cause of the discrepancy. These are the first successful Langley calibrations of filter radiometers at 300 nm and 305 nm of which we are aware. The Langley calibration factors with the radiometer in the shadow-band mode for the all channels agree with those derived from lamps from 0% difference to at worst 7% higher at 300 nm for radiometer 393 using lamp 96598. The uncertainty due to the radiometer signal to noise is smaller using the Langley method than during

lamp calibrations, which constitutes a major advantage of UV Langley calibrations for these radiometers.

There are no significant differences in Langley calibration factors when the radiometer was in the shadow-band configuration compared to when it was on the Sun tracker except for the 300 nm channel on radiometer 282. This suggests that in the UV the shadow band is equally effective as the Sun tracker in isolating the direct beam.

The sources of uncertainty are as follow:

(1) absolute calibration uncertainty in the extraterrestrial solar flux; different measurements will be compared in the future; (2) absolute calibration uncertainty in the FEL lamps used to calibrate UV-MFRSR; (3) repeatability of radiometer voltages when under lamp calibration; (4) repeatability of the Langley voltage intercepts; at the shortest wavelengths this is caused by variations in ozone optical depth during the Langley event; this is evident in the relatively large standard errors on the mean for the 300 nm and 305 nm channels; screening the Langley events to exclude days when ozone is changing rapidly will be investigated; and (5) corrections for finite filter bandwidth and ozone air mass factors.

This study shows that the Langley method shadow-band UV radiometers at a high altitude site is an effective method of obtaining calibrations which approaches the accuracy of those from lamps. Advantages over lamp calibrations include superior signal-to-noise, automated operation, no loss of instruments operation, and reference to an absolute, nearly unchanging standard that is universally available. Used together with lamp calibrations, the Langley method provide continual checks of radiometer and lamp stability. The advantage of a shadow band over a Sun-tracker radiometer is that in addition to the direct beam the shadow band retrieves global and diffuse irradiances.

The Tropospheric Ultraviolet and Visible (TUV v3.9) radiation model is available at <http://www.acd.ucar.edu>, by following the modeling link. The SUSIM ATLAS 3 high-resolution (0.15 nm FWHM) solar spectrum for November 13, 1994, is publically available at the ftp site: [susim.nrl.navy.mil](ftp://susim.nrl.navy.mil), [cd pub.atlas3](ftp://cd.pub.atlas3). For assistance, send e-mail to Dianne Prinz at prinz@susim.nrl.navy.mil.

Acknowledgments. We thank John DeLuisi and Beat Schmid for helpful discussions about their UV research. The outstanding logistical support of the Mauna Loa Observatory operated by the Climate Monitoring Diagnostic Laboratory of the National Oceanic and Atmospheric Administration and especially the help of its director Russ Schnell is greatly appreciated. Thanks to two anonymous reviewers whose thoughtful comments resulted in an improved paper. This paper is dedicated to Knut Stamnes and Glenn Shaw.

References

- Barlow, R. J., *Statistics: A Guide to the Use of Statistical Methods in the Physical Sciences*, 204 pp., John Wiley, New York, 1989.
- Bigelow, D. S., J. R. Slusser, A.F. Beaubien, and J. H. Gibson, The USDA Ultraviolet Radiation Monitoring Program, *Bull. Am. Meteorol. Soc.*, 79, 601-615, 1998.
- Bigelow, D. S., and J. R. Slusser, Establishing the stability of multifilter UV rotating shadow-band radiometers, *J. Geophys. Res.*, this issue.
- Early, E. A., et al., The 1995 North American Interagency Intercomparison of ultraviolet monitoring spectroradiometers, *J. Res. Natl. Inst. Stand. Technol.*, 103, 15-62, 1998a.
- Early, E. A., E. A. Thompson, and P. Disterhoft, Field calibration unit for ultraviolet spectroradiometers, *Appl. Opt.*, 37, 6664-6670, 1998b.
- Forgan, B. W., Bias in solar constant determination by the Langley method due to structured aerosol: Comment, *Appl. Opt.*, 27, 2546-2548, 1988.
- Gröbner, J., M. Blumthaler, and W. Ambach, Experimental investigation of spectral global irradiance measurements errors due to non-ideal cosine response, *Geophys. Res. Lett.*, 23, 2493-2496, 1996.
- Harrison, L., and J. Michalsky, Objective algorithms for the retrieval of

- optical depths from ground-based measurements, *Appl. Opt.*, *33*, 5126-5132, 1994.
- Harrison, L., J. Michalsky, and J. Berndt, Automated multi-filter rotating shadow band radiometer: An instrument for optical depth and radiation measurements, *Appl. Opt.*, *33*, 5118-5125, 1994.
- Houghton, H. G., *Physical Meteorology*, 442 pp., MIT Press, Cambridge, Mass., 1985.
- Kasten, F., and A. Young, Revised optical air mass tables and approximate formula, *Appl. Opt.*, *28*, 4735-4738, 1989.
- Kiedron, P. W., J. J. Michalsky, J. L. Berndt, and L. C. Harrison, Comparison of spectral irradiance standards used to calibrate shortwave radiometers and spectroradiometers, *Appl. Opt.*, *38*, 2432-2439, 1999.
- Komhyr, W. D., Operations handbook—Ozone observations with a Dobson spectrophotometer, *WMO Global Ozone Res. Monit. Proj. Rep. 6*, World Meteorol. Organ., Geneva, 1980.
- Lean, J. L., G. J. Rottman, H. L. Kyle, T. N. Woods, J. R. Hickey, and L. C. Puga, Detection and parameterization of variations in solar middle and near-ultraviolet radiation (200-400 nm), *J. Geophys. Res.*, *102*, 29,939-29,956, 1997.
- Madronich S., UV radiation in the natural and perturbed atmosphere, in *Environmental Effects of Ultraviolet (UV) Radiation*, pp. 17-69, A. F. Lewis, New York, 1993.
- McKenzie, R. L., and P. V. Johnston, Comment on "Problems of UV-B radiation measurements in biological research: Critical remarks on current techniques and suggestions for improvements" by H. Tüg and M. E. M. Baumann, *Geophys. Res. Lett.*, *22*, 1157-1158, 1995.
- Schmid, B., and C. Wehrli, Comparison of Sun photometer calibration by use of the Langley technique and the standard lamp, *Appl. Opt.*, *34*, 4500-4512, 1995.
- Schmid, B., P. R. Spyak, S. F. Biggar, C. Wehrli, J. Sekler, T. Ingold, C. Matzler, and N. Kampfer, Evaluation of the applicability of solar and lamp radiometric calibrations of a precision Sun photometer operating between 300 and 1025 nm, *Appl. Opt.*, *37*, 3923-3941, 1998.
- Shaw, G. E., Solar spectral irradiance and atmospheric transmission at Mauna Loa Observatory, *Appl. Opt.*, *21*, 2007-2011, 1982.
- Slusser, J.R., J. H. Gibson, D. S. Bigelow, D. Kolinski, W. Mou, G. Koenig, and A. Beaubien, Comparison of column ozone retrievals employing a UV multi-filter rotating shadow-band radiometer with those from Brewer and Dobson spectrophotometers, *Appl. Opt.*, *38*, 1543-1551, 1999.
- Stamnes, K., S.C. Tsay, W. Wiscombe, and K. Jayaweera, Numerically stable algorithm for discrete-ordinate-method radiative transfer in multiple scattering and emitting layered media, *Appl. Opt.*, *27*, 2502-2509, 1988.
- Thomason, L. W., B. M. Herman, and J. A. Reagan, The effect of atmospheric attenuators with structured vertical distributions on air mass determinations and Langley plot analysis, *J. Atmos. Sci.*, *40*, 1851-1854, 1983.
- Tomasi, C., V. Vitale, and L. V. De Santis, Relative optical mass functions for air, water vapour, ozone, and nitrogen dioxide in atmospheric models presenting different latitudinal and seasonal conditions, *Meteorol. Atmos. Phys.*, *65*, 11-30, 1998.
- Tüg, H., and M. Baumann, Problems of UV-B radiation measurements in biological research: Critical remarks on current techniques and suggestions for improvements, *Geophys. Res. Lett.*, *21*, 689-692, 1994.
- Wilson, S.R. and B.W. Forgan, In situ calibration technique for UV spectral radiometers, *Appl. Opt.*, *34*, 5475-5484, 1995.

D. Bigelow, J. Gibson, and J. Slusser, USDA UV-B Radiation Monitoring Program, Natural Resource Ecology Laboratory, Colorado State University, Fort Collins, CO 80523 (sluss@nrel.colostate.edu).

D. Kolinski, High Altitude Observatory, National Center for Atmospheric Research, Boulder, CO 80301.

P. Disterhoft and K. Lantz, Surface Radiation Research Branch, NOAA Air Resource Laboratory, Boulder, CO 80303.

A. Beaubien, Yankee Environmental Systems, Turners Falls, MA 01376.

(Received February 16, 1999; revised May 19, 1999; accepted June 7, 1999.)

¹USDA UV-B Radiation Monitoring Program, Natural Resource Ecology Laboratory, Colorado State University, Fort Collins.

²Now at the High Altitude Observatory, National Center for Atmospheric Research, Boulder, Colorado.

³Surface Radiation Research Branch, NOAA Air Resource Laboratory, Boulder, Colorado.

⁴Yankee Environmental Systems, Turners Falls, Massachusetts.

Copyright 1999 by the American Geophysical Union.

Paper number 1999JD9004510.
0148-0227/99/1999JD900451509.00

Figure 1. Langley plot for the 300 nm channel from radiometer 282 in the shadow-band configuration for March 1, 1998. The optical depth at this wavelength is 3.348. Measurements are 3 min averages of 20 s snapshots.

Figure 2. Dimensions of the collimating tube and apertures that define the field-of-view for the Sun tracking radiometer. The full field of view determined by $\theta = \arctan A/L$ was initially 2.0° and finally 1.5° . The internal baffles limit scattered light within the tube.

Figure 3. Ratio of Langley to lamp calibration factors for radiometer 282 on tracker with 2.0° field of view and in the shadow-band configuration.

Figure 4. Ratio of Langley to lamp calibration factors for radiometer 393 on tracker with a 2.0° and 1.5° field of view and in the shadow-band configuration.

Figure 5. Histogram of 133 $V_{o,\lambda}$ values for radiometer 282 in the shadow-band mode from March 1 to September 30, 1998. A Gaussian distribution is overlaid on the histogram.

Figure 6. A comparison of lamp 96599 irradiance at 50.0 cm compared with the solar irradiance generated from a model with column ozone=280 DU, $SZA=63^\circ$, altitude=3.4 km, aerosol optical depth=0.05, and surface albedo=0.02. Since each channel is optimized for the solar irradiance, there will be insufficient signal to noise at the longer-wavelength channels when calibrated by the lamp method.

Table 1. Corrections to V_o Due to Finite Bandpass and Ozone Air Mass Factors (AMF)

Wavelength (nm)	Finite Bandpass	Ozone AMF
300	1.1017	0.9558
305	1.0222	0.97876
312	1.0086	0.9902
318	1.0031	0.99592
326	1.0009	0.999
332	1	1
368	1	1

Table 2. Configuration of Radiometers at MLO 1998 Including Number of Good Plots at 300 nm Shown in Parentheses

Radiometer	Jan. 1 to Feb. 27	March 1 to April 18	June 17 to Sept. 30
282	tracker 2.0° (45)	shadow band (41)	shadow band (77)
393	shadow band (50)	tracker 2.0° (31)	tracker 1.5° (56)

Table 3. Number of Good Langley Plots and Those $> \pm 2\sigma$ for Radiometers 282 and 393 for Entire Experiment

λ	282		393	
	Good Plots	$> \pm 2\sigma$	Good Plots	$> \pm 2\sigma$
300	180	11	148	8
305	195	2	160	10
311	190	7	161	7
317	187	9	164	5
325	186	9	164	4
332	184	9	163	5
368	181	9	164	39

Table 4. Estimated Percent Drift of Radiometer 282 Over 213 Days During 1998

λ	Percent Drift Over 213 Days
300	-0.2
305	0.1
311	-1.3
317	-1.3
325	-0.1
332	-0.8
368	1.3

Table 5. Average Voltage Intercepts (mV) and Standard Deviation, σ , (%) for Radiometer 282

λ (nm)	Tracker 2.0°		Shadow Band March 1 to April 18		Shadow Band June 17 to Sept. 30	
		σ (%)		σ (%)		σ (%)
300	53365	4.4	52318	2.9	52634	2.2
305	16566	2.4	16625	2.4	16676	1.9
311	6376	1	6466	1.8	6404	1.1
318	2803	1.3	2838	1.5	2802	1.1
325	3654	1.3	3690	1.2	3689	1.1
332	2573	0.6	2567	1.2	2593	1.1
368	1792	0.5	1816	1	1837	0.9

Table 6. Average Voltage Intercepts (mV) and Standard Deviation, σ , (%) for Radiometer 393

λ (nm)	Shadow-	σ (%)	Tracker 2.0°		Tracker 2.0°	
	Band		σ (%)	σ (%)	σ (%)	σ (%)
300	54920	4.4	59456	4.6	58972	3.1
305	20912	2.3	21472	2.1	21164	1.6
311	4717	1.6	4785	2	4812	1.4
318	2437	1.2	2457	1.4	2466	1.3
325	2649	1.2	2673	1.2	2679	1.2
332	1901	1.2	1931	2.3	1937	1.3
368	1686	1.1	1687	1.4	1688	0.8

Table 7. Comparison of Lamp to Langley Shadow-Band Calibration Factors ($W / m^2 / nm / V$) for Radiometer 282

Radiometer 282 λ (nm)	Lamp Calibration 96598	Lamp Calibration 96599	Langley Calibration Shadow Band
300	$8.4942 \cdot 10^{-3}$	$8.5120 \cdot 10^{-3}$	$8.7695 \cdot 10^{-3}$
305	$3.6136 \cdot 10^{-2}$	$3.6475 \cdot 10^{-2}$	$3.6356 \cdot 10^{-2}$
311	$1.0644 \cdot 10^{-1}$	$1.0903 \cdot 10^{-1}$	$1.0908 \cdot 10^{-1}$
318	$2.5602 \cdot 10^{-1}$	$2.5435 \cdot 10^{-1}$	$2.5895 \cdot 10^{-1}$
325	$2.4768 \cdot 10^{-1}$	$2.4923 \cdot 10^{-1}$	$2.4968 \cdot 10^{-1}$
332	$3.6778 \cdot 10^{-1}$	$3.7182 \cdot 10^{-1}$	$3.8131 \cdot 10^{-1}$
368	$6.3000 \cdot 10^{-1}$	$6.3382 \cdot 10^{-1}$	$6.5098 \cdot 10^{-1}$

Table 8. Comparison of Lamp to Langley Shadow Band Calibration Factors ($W / m^2 / nm / V$) for Radiometer 393

Radiometer 393 λ (nm)	Lamp Calibration 96598	Lamp Calibration 96599	Langley Calibration Shadow Band
300	$7.8729 \cdot 10^{-3}$	$7.8681 \cdot 10^{-3}$	$8.4173 \cdot 10^{-3}$
305	$2.7080 \cdot 10^{-2}$	$2.7706 \cdot 10^{-2}$	$2.8791 \cdot 10^{-2}$
311	$1.4020 \cdot 10^{-1}$	$1.4731 \cdot 10^{-1}$	$1.4990 \cdot 10^{-1}$
318	$2.8631 \cdot 10^{-1}$	$2.9675 \cdot 10^{-1}$	$3.0256 \cdot 10^{-1}$
325	$3.2944 \cdot 10^{-1}$	$3.4739 \cdot 10^{-1}$	$3.4043 \cdot 10^{-1}$
332	$4.8741 \cdot 10^{-1}$	$5.0705 \cdot 10^{-1}$	$5.1725 \cdot 10^{-1}$
368	$6.7142 \cdot 10^{-1}$	$6.9184 \cdot 10^{-1}$	$7.0246 \cdot 10^{-1}$

Table 9. Radiometer 282 Ratio of Langley Shadow Band to Lamp Calibrations

Channel (nm)	300	305	311	318	325	332	368
Lamp 96598	1.032	1.006	1.025	1.011	1.008	1.037	1.033
Lamp 96599	1.032	0.997	1	1.018	1.002	1.026	1.027

Table 10. Radiometer 393 Ratio of Langley Shadow Band to Lamp Calibrations

Channel (nm)	300	305	311	318	325	332	368
Lamp 96598	1.069	1.063	1.069	1.057	1.033	1.061	1.046
Lamp 96599	1.07	1.039	1.018	1.02	0.988	1.02	1.015

Table 11. Uncertainties for Multiple Langley Calibrations

Factor	Accuracy	Repeatability
Measured spectral response function of each channel	$\pm 0.5\%$	$\pm 0.5\%$
Repeatability of Langley voltage intercept	$\pm 0.6\%$ $\pm 0.2\%$	$\pm 0.6\%$ at 300 nm $\pm 0.2\%$ at 368 nm
Uncertainty in extraterrestrial solar irradiance	$\pm 2.0\%$	$\pm 0.5\%$
Correction for finite bandpass	$\pm 3.0\%$ $\pm 0.0\%$	$\pm 3.0\%$ at 300 nm $\pm 0.0\%$ at 368 nm
Correction for ozone air mass factor	$\pm 1.0\%$ $\pm 0.0\%$	$\pm 1.0\%$ at 300 nm $\pm 0.0\%$ at 368 nm
Total uncertainty	$\pm 3.8\%$ $\pm 2.1\%$	$\pm 3.3\%$ at 300 nm $\pm 0.7\%$ at 368 nm

Table 12. Uncertainties for Lamp Calibrations

Factor	Uncertainty
Measured spectral response function of each channel	$\pm 0.5\%$
Lamp irradiance (secondary standard)	$\pm 1.0\%$
Interpolation uncertainty	$\pm 0.4\%$
Dark voltage subtraction	$\pm 1.0\%$
Repeatability of radiometer voltage	± 2.0
Total uncertainty	$\pm 2.5\%$ at for all channels

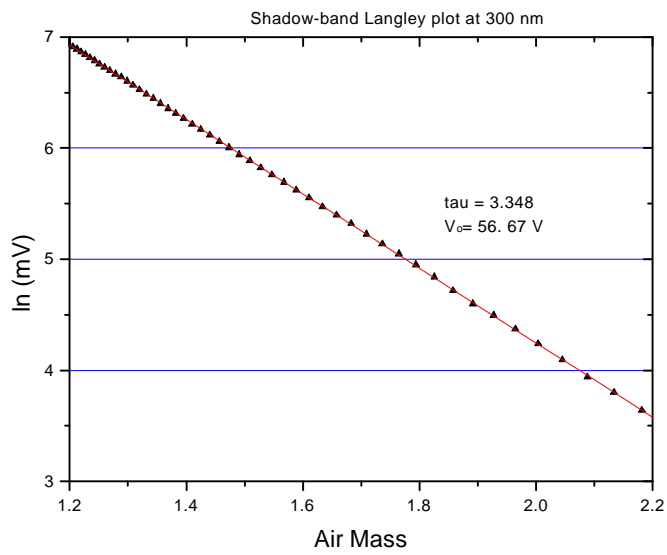
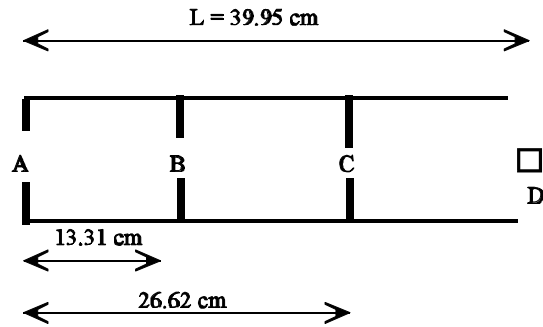


Figure 1: Langley plot for the 300 nm channel from radiometer 282 in the shadow-band configuration for March 1, 1998. The optical depth at this wavelength is 3.348. Measurements are 3-minute averages of 20 second snapshots.



Diameters
 Aperture A: 1.40 cm (initial) 1.05 cm (final)
 Aperture B: 1.22 cm
 Aperture C: 1.04 cm
 Diffuser D: 0.89 cm

Figure 2: Dimensions of the collimating tube and apertures that define the field-of-view for the Sun-tracking radiometer. The full field-of-view determined by $\theta = \arctan A/L$ was initially 2.0° and finally 1.5° . The internal baffles limit scattered light within the tube.

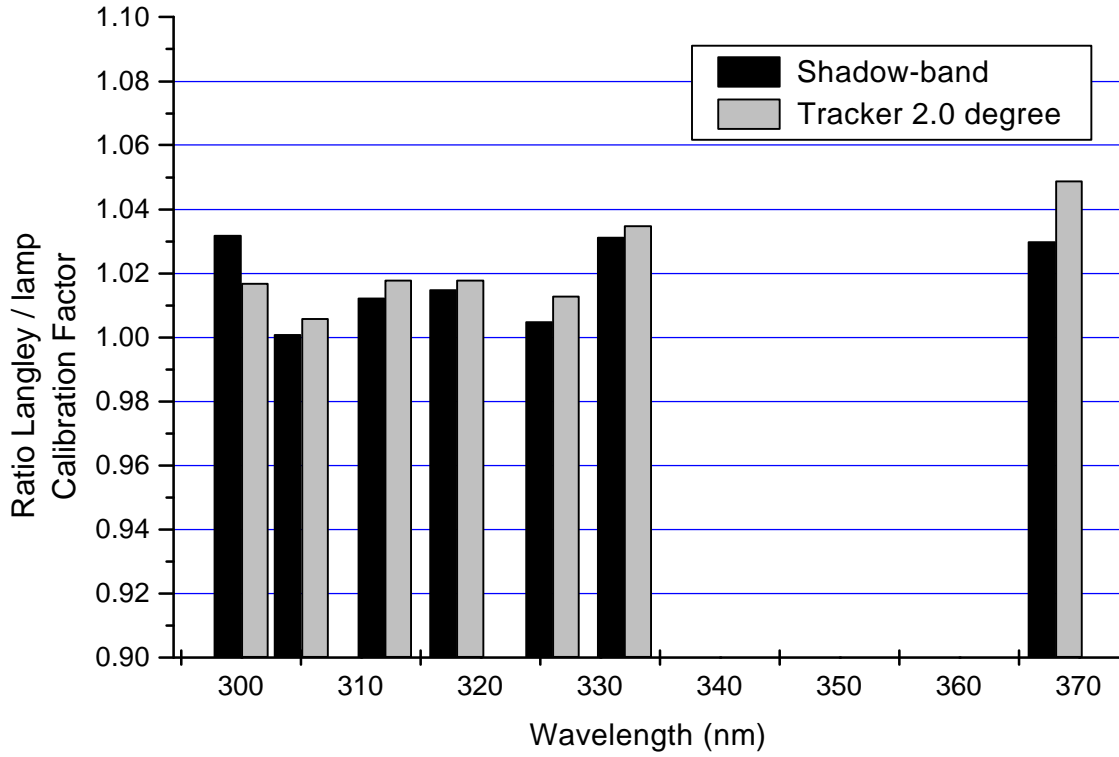


Figure 3: Ratio of Langley to lamp calibration factors for radiometer 282 on tracker with a 2.0° field-of-view, and in the shadow-band configuration.

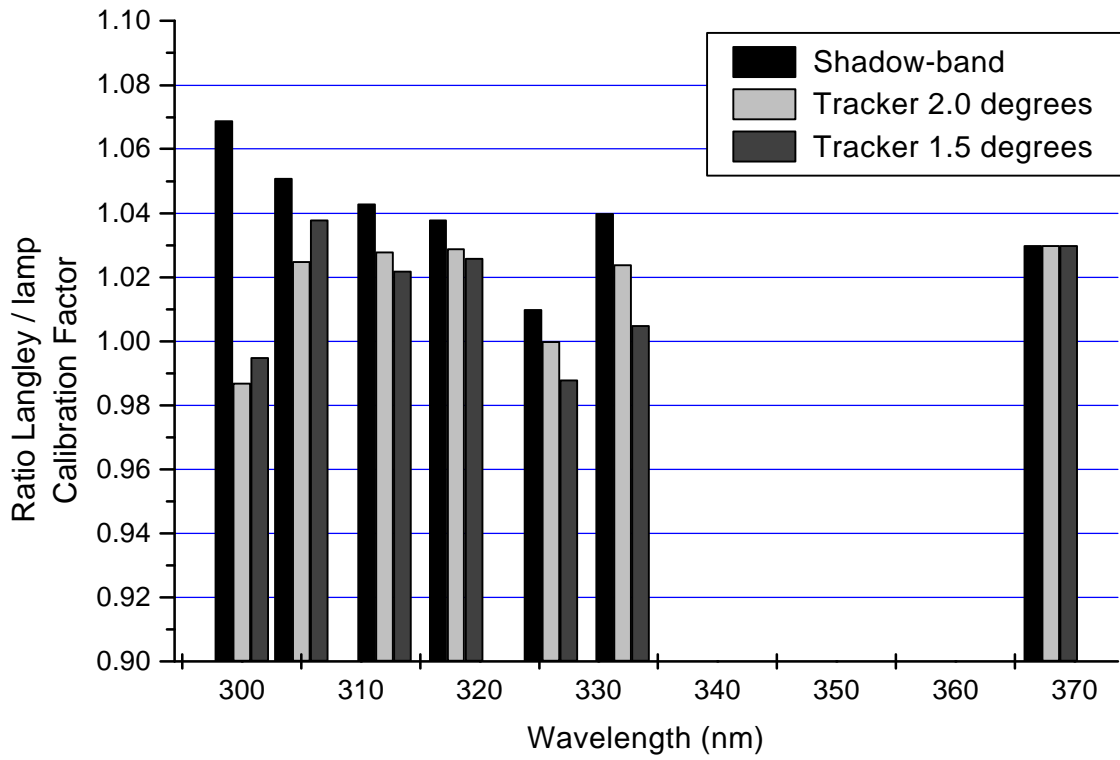


Figure 4: Ratio of Langley to lamp calibration factors for radiometer 393 on tracker with a 2.0° and 1.5° field-of-view, and in the shadow-band configuration.

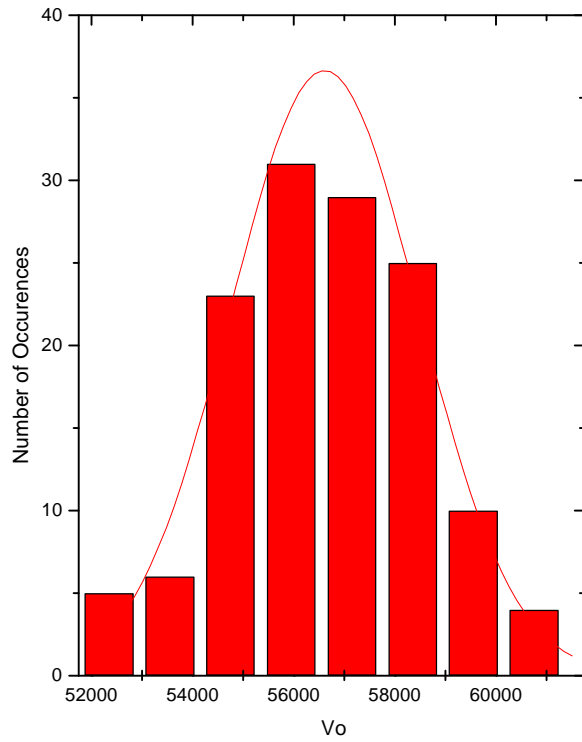


Figure 5: Histogram of 133 V_o values at 300 nm for the period March 1 through September 30, 1998 for radiometer 282 in the shadow-band mode. A Gaussian distribution is overlaid on the histogram

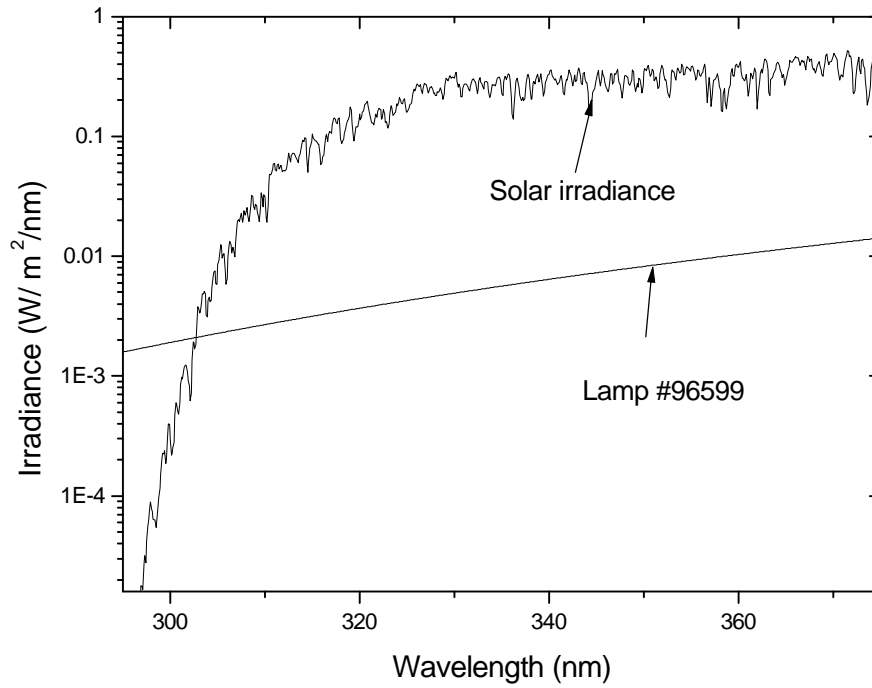


Figure 6 A comparison of lamp #96599 irradiance at 50.0 cm compared with the Solar irradiance generated from a model with column ozone=280 DU, SZA=63°, altitude=3.4 km, aerosol optical depth=0.05, and surface albedo=0.02. Since each channel is optimized for the Solar irradiance, there will be insufficient signal-to-noise at the longer wavelength channels when calibrated by the lamp method.